Dynamic Motion Residuals in Swath Sonar Data : Ironing out the Creases

John E. Hughes Clarke
Ocean Mapping Group
Dept. Geodesy and Geomatics Engineering
University of New Brunswick
Canada
jhc@omg.unb.ca

Abstract

As the component sensors in swath sonar systems have improved, the focus on total system performance has turned increasingly to the remaining imperfections in the system integration. Of particular concern is that faint but systematic across track ribbing often remains in otherwise high-quality data.

Traditional field calibration procedures primarily look for the signature of static systematic error contributions. These procedures (the conventional patch test) only examine a subset of the possible systematic biases in the configuration of an integrated swath sonar system. Other systematic biases can cause dynamic rather than static signatures in the resulting bathymetric data.

These dynamic errors can be separated into those that produce errors that vary with periods in the ocean wave spectrum (most commonly referred to as the “wobbles”) and those whose period is dictated by the long period accelerations of the vessels (turns and other course changes, obstacle avoidance and speed changes).
Herein the theory behind the cause for a number of common wobble sources is examined. For the case of shallow water surveys, where the ping period is short with respect to the typical wave period, the wobble signatures can be easily discerned. The differences in the signatures of each of the wobbles are highlighted allowing rapid classification and thus a means of removal of the underlying systematic bias.

Introduction

Swath bathymetric sonar systems represent an integration of a variety of acoustic and ancillary sensors. Proper relative alignment, location and time synchronization of the sensor suite is an essential prerequisite to obtaining high quality bathymetric data.

Gross integration errors are normally glaringly obvious and are trivial to remove. A more insidious problem, however, is the faint (usually within error specifications) but pervasive across track ribbing that permeate many swath sonar surveys. This ribbing is normally not visible with traditional display methods (sounding plots, contours or colour coding) but show up strongly with the aid of surface slope derivative maps (most commonly sun shading) that are increasingly being generated (Fig. 1). These ribs or "wobbles" have come to be an issue of contention in many cases between clients and contractors (Hughes Clarke, 2000).

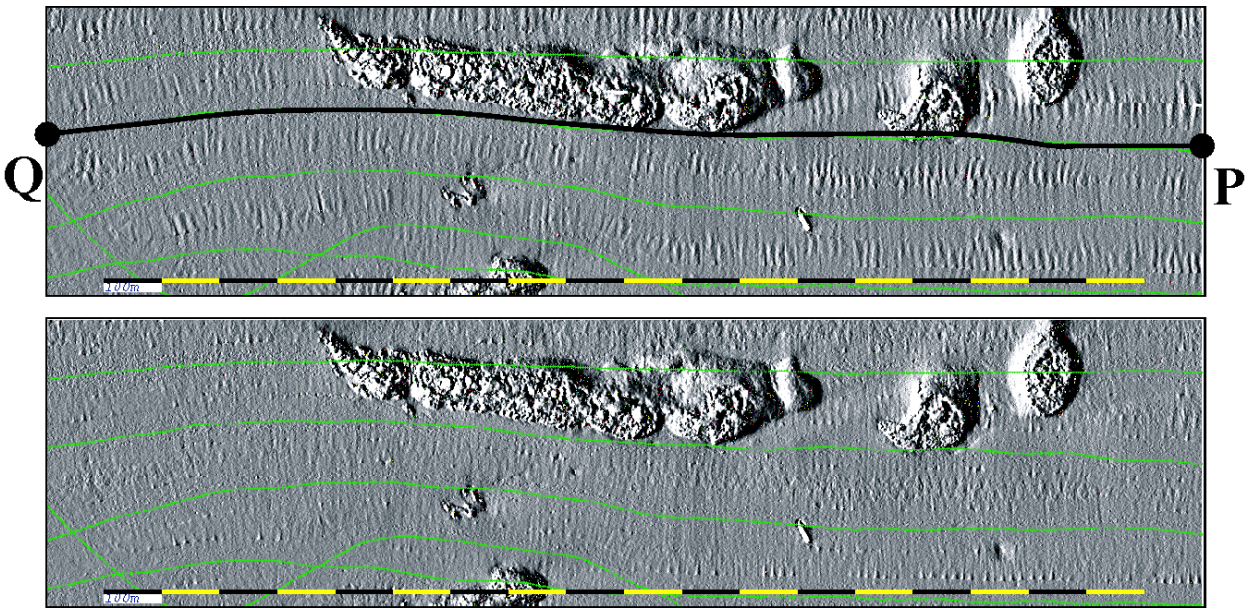

Figure 1*: sun-illuminated terrain models of EM1002 bathymetric data in 30m of water. The top image shows data as originally collected with pronounced ship-track orthogonal ribbing. The bottom plot shows data after shifting the motion time series by –20ms.*
The peak to peak magnitude of the apparent rippling is on the order of +/- 1.0-1.5% (well within the required standard – IHO order 2). Data courtesy of the Geological Survey of Israel.

This paper aims to explain the underlying causes behind the common types of ribbing, so that the user can more easily identify the signature of different error sources and subsequently correct the data.

Basic Alignment

The most basic alignment method is commonly referred to as the Patch Test. It was originally developed in the early 1970's in support of classified deep-water multibeam sonar systems and first publicly described as part of NOAA mapping operations in the 1980's (Herlihy et al., 1989 and Hillard and Rulon, 1989). This test examines the repeatability of the system over a pre-defined patch of the seafloor. By comparing the

relative gradient and alignment of regional slopes and targets when imaged from different directions and/or different speeds, inferences may be made about a number of integration errors.

.

The conventional patch test examines the following:

- relative heading misalignment between the active sonar and the heading sensor,
- relative pitch misalignment between the active sonar and the pitch sensor,
- relative roll misalignment between the active sonar and the roll sensor and
- relative time mis-synchronisation between the position solutions and the sonar clock

The test assumes the following :

1. That alignment of the heading, pitch and roll sensors with respect to the ship's coordinate system is already known.
2. That the relative offsets of all sensors is already known in the ships coordinate system.
3. That other timing mis-synchronisations (for example between sonar and the source of roll/pitch and heading) are inconsequential
4. That the surface sound speed is known and therefore the beam steered angles with respect to the sonar reference frame are well described.
5. That the water column sound speed profile is adequately known.
6. That the performance of the roll, pitch and heading sensors are not significantly influenced by vessel dynamics and can capture the full spectrum of ship motions.

These assumptions however, are not always the case and thus they may cause additional sources of error. Failings in any of these can result in both a constant bias and/or time varying error in the resulting swath bathymetric data set.

Critical aspects of these assumptions and their limitations will herein be examined. Specific attention will be paid to those that are common sources of dynamic motion error. But first we need to examine how a dynamically varying error manifests itself in swath sonar data.

Manifestation of dynamic error residuals in Swath Sonar Data

All of the integration error types (which will be described in detail below) generate time varying errors in either the position or orientation of the sonar. The characteristic time period over which the errors will change reflects the driving signatures that are centred primarily within the ocean wave spectra.

It should be noted that there are a whole other family of dynamic errors related to motion sensors limitations which are distinct from the ones discussed here (not a result of

imperfect integration). The two main examples are slowly drifting position or orientation errors related to filter time constants and imperfect definition of ultra-long wave periods (generally over 15 seconds) due to limited bandwidth capabilities of the motion sensors. These are distinct from the errors described here in that they lie outside the usual wave spectra and will not be discussed herein.

There is always a finite period over which the transmission and reception cycle takes place. Over that time period, because the magnitude of the error is not constant, the effect of the error on each bottom detection will be slightly different. As long, however, as the ping period is short with respect to the driving signature (normally ocean wave spectra in the 4-12 second period range) then the magnitude of the error will appear as if it were constant for each shot. For example if the maximum slant range is less than 75m (e.g. 35m depth with a ~120° swath) ping frequency should be above 10 Hz, 2 orders of magnitude above the typical ~0.1Hz of ocean waves.

Under these conditions, as the error varies insignificantly throughout the ping cycle, the mean instantaneous across track profile should be overprinted with a sample of the magnitude of the angular and/or position error within the time window of the transmit/receive cycle (Fig. 2).

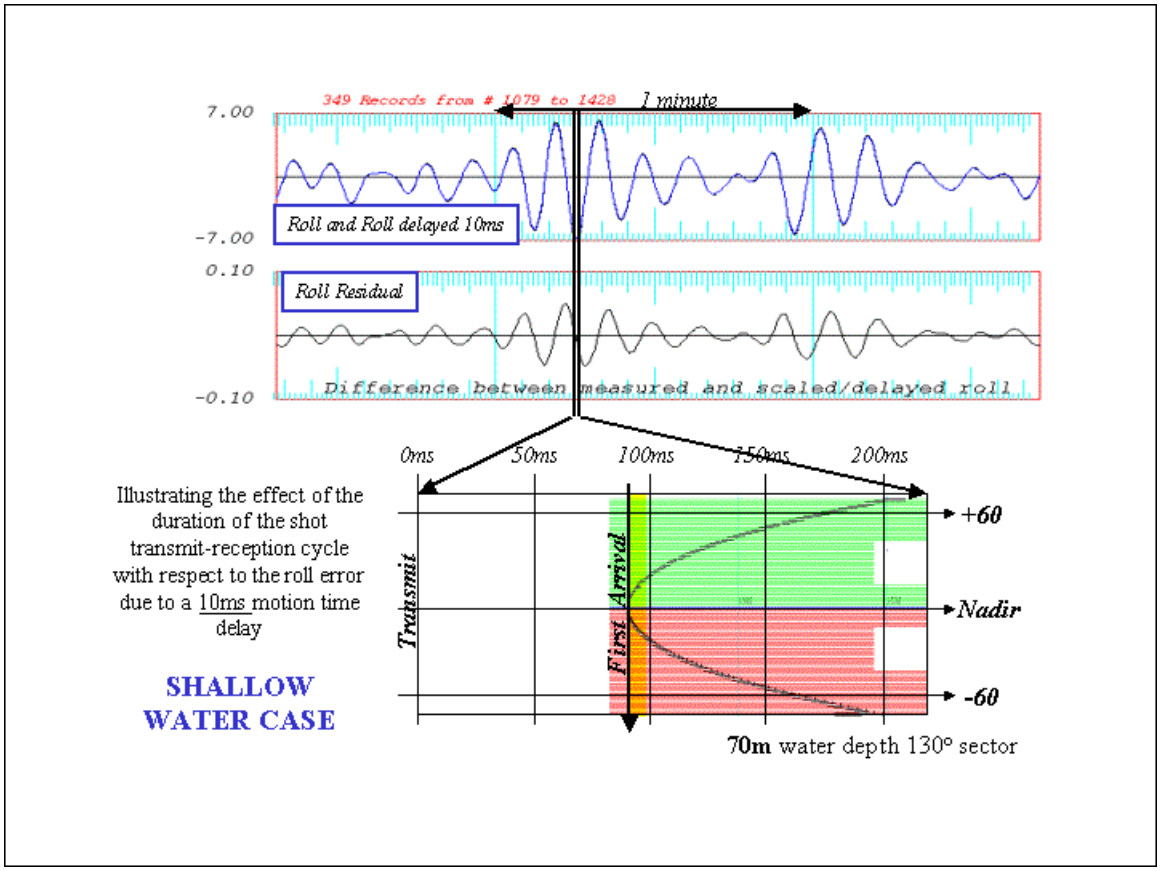

Figure 2: *Upper: showing a typical roll time series, delayed by 10ms and the resulting time series of roll error. Note that the error contains a similar spectral characteristic to the driving signature.*
Lower: showing a typical receive cycle of one ping of a multibeam sonar. The parabolic arc represents the location of the individual bottom detection solutions as a function of two-way travel time and sonar-relative

angle. In this case, with a seafloor depth of 70m, the entire shot-reception cycle takes place within ~ 200ms during which time the roll error magnitude hardly changes.

Nevertheless, from ping to ping, as the error magnitude slowly changes the manifestation in the data will also slowly change and should be reflected in a slow change in the apparent character of the seafloor (Fig. 3). For example if a roll error was changing from +/- 0.5 ° over a 6 second period, the seafloor would rock back and forward similarly. This would appear as an across track ribbing in the swath sonar data (Fig. 3) superimposed upon the natural variation in the seafloor topography. We thus have the potential to extract the error time series (see later section) for analysis.

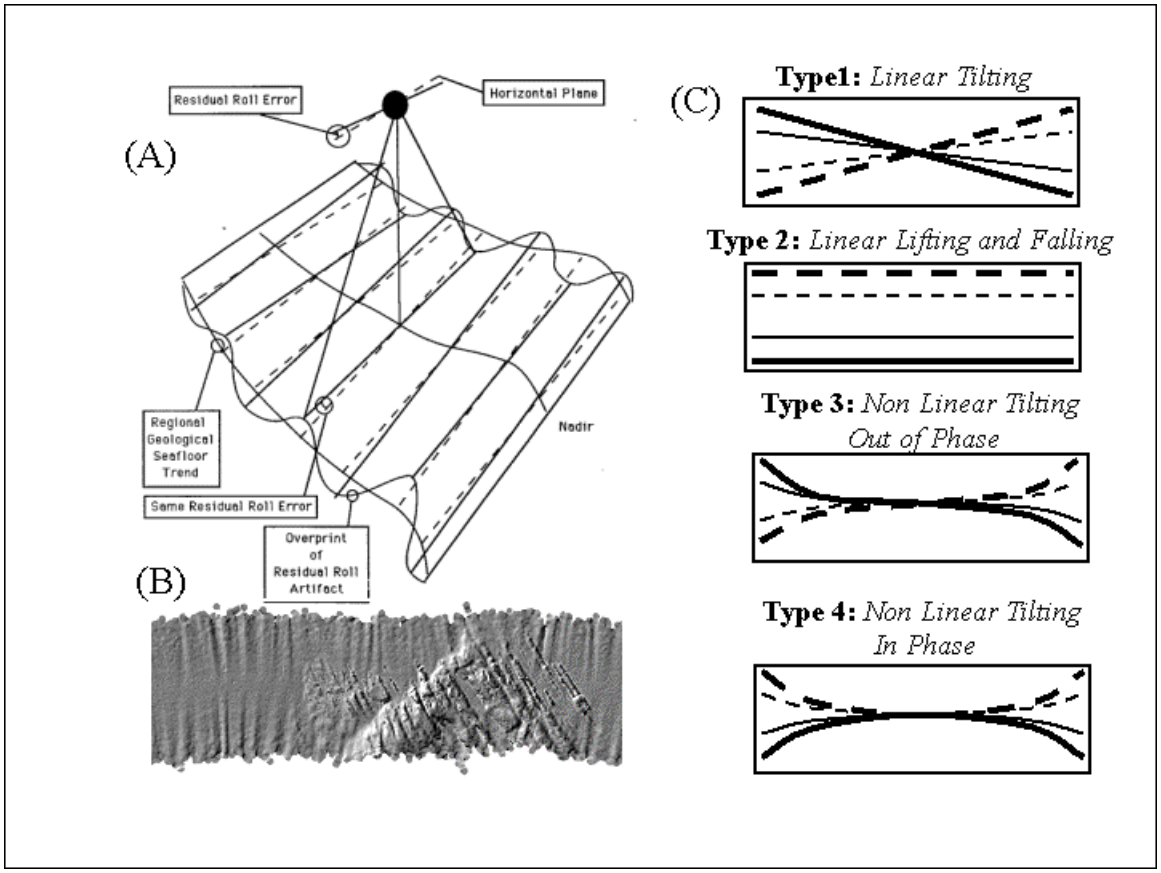

Figure 3*: (A): Showing the overprinting of the roll error time series on the natural seafloor slope variability. (B): sun-illuminated terrain model of a single swath of multibeam data passing from smooth to rough seafloor in which the roll error signature can easily visually be distinguished from the natural relief by the fact that is is always orthogonal to the ships-track. (C): showing the 4 main manifestations of across-track ribbing. These characteristic error manifestations (referred to as types I-IV), are explained in more detail later in the text.*

As one moves into deeper water, however, where the pulse repetition period approaches the characteristic error period (Fig . 4), the error is now, different for each of the beams. Thus, for the case of a simple roll error, the error would progressively change over the receive cycle.

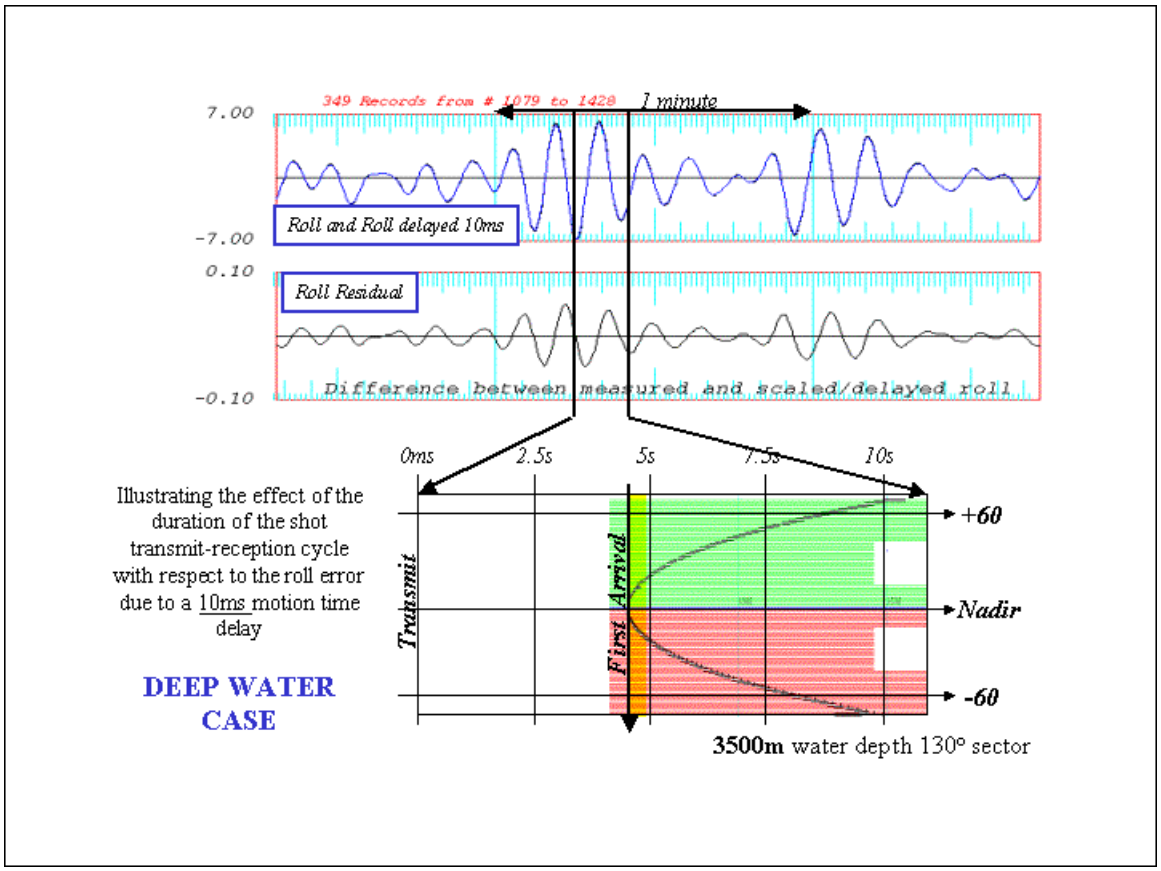

Figure 4*: same layout as figure 2 except now the ping cycle represents a multibeam ping in 3,500m of water with a shot cycle of over 10 seconds. In this case the magnitude and sign of the roll error clearly change over the reception cycle.*

As a result rather than a single ping exhibiting a tilt characteristic of a single instant of the roll error, it would have a ripple overprinted as the magnitude and sign of the error changes through the reception cycle. As the ping period grows with increasing water depth (Fig. 5), the approximation of the across track slope as an indicator of the instantaneous roll error gets worse. The analyses presented herein are only generally useful where ping period is < 10% of characteristic wave period.

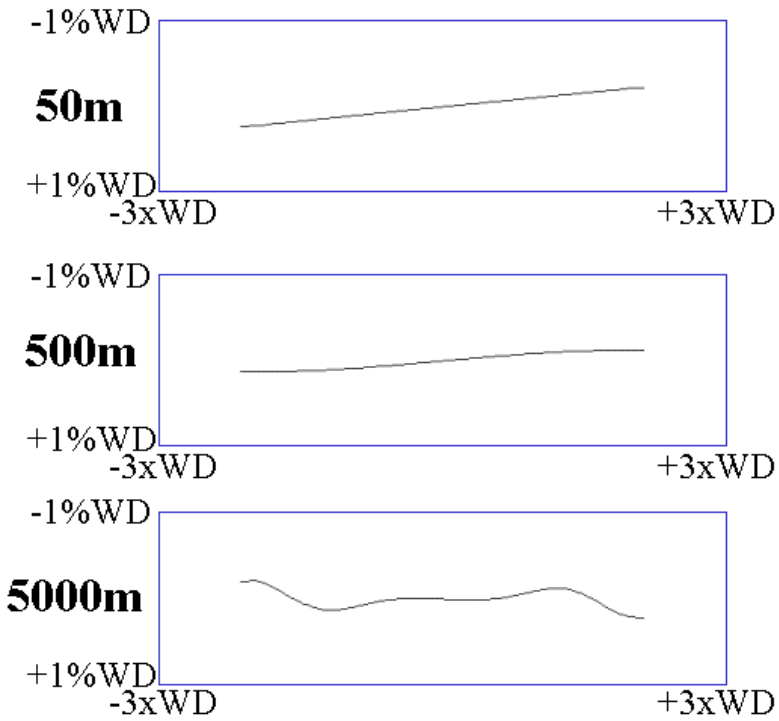

Figure 5*: three examples of a single ping of a multibeam sonar acquired over a flat seafloor that is corrupted by a dynamic motion residual (for this example, a roll error, generated by a 50ms time delay on a 6 second period, +/-2° roll). WD = water depth.*
In the shallow-water case (top) the error manifests itself as a linear tilt to the swath, whereas in the deep-water case (lower) it is manifested as a ripple migrating out through the swath, near symmetrically on either side, At intermediate depths (middle), the swath takes on a nonlinear curved profile.

Error Sources

Seven of the most common different integration problems that produce dynamic motion residuals will herein be examined in turn. Whilst there are several other integration problems, these seven are specifically selected as they are the most common ones routinely analysed by the author.

In order to graphically illustrate the impact and characteristic signature of each motion residual, a simulator has been developed that allows the user to generate synthetic swath data from a sonar of their choice (in this case, a 150°, roll-stabilised, equi-distant beam spacing system operating at 8 knots). The model can be run for a user specified depth range, within which the regional slope dip and strike vary slowly. For this corridor of user specified data, a simulated (Fig. 6) or an actual (Fig. 7) motion time series has been applied and the effect of each one of the seven biases added. The end result is a series of sun-illuminated terrain models (Figs. 6 and 7), which represent a pictogram showing the primary correlation of the dynamic residuals and the motion time series.

For clarity, an idealized time series is used in figure 6 in which packets of roll, pitch or heave only occur discretely so that unambiguous correlation can be done. For real data of course, the roll pitch and heave data are usually highly correlated. However, if one examines any natural time series (Fig 7 lower) one sees that there are always short characteristic periods in which one of the three motions dominates. By examining the correlation of the motion residuals with burst energy events in one of the three motion types one can usually visually see if the two are correlated. In order to even better isolate the effect of each driving signature of course, one can steam across the swell to emphasize roll and then into the swell to emphasize pitch.

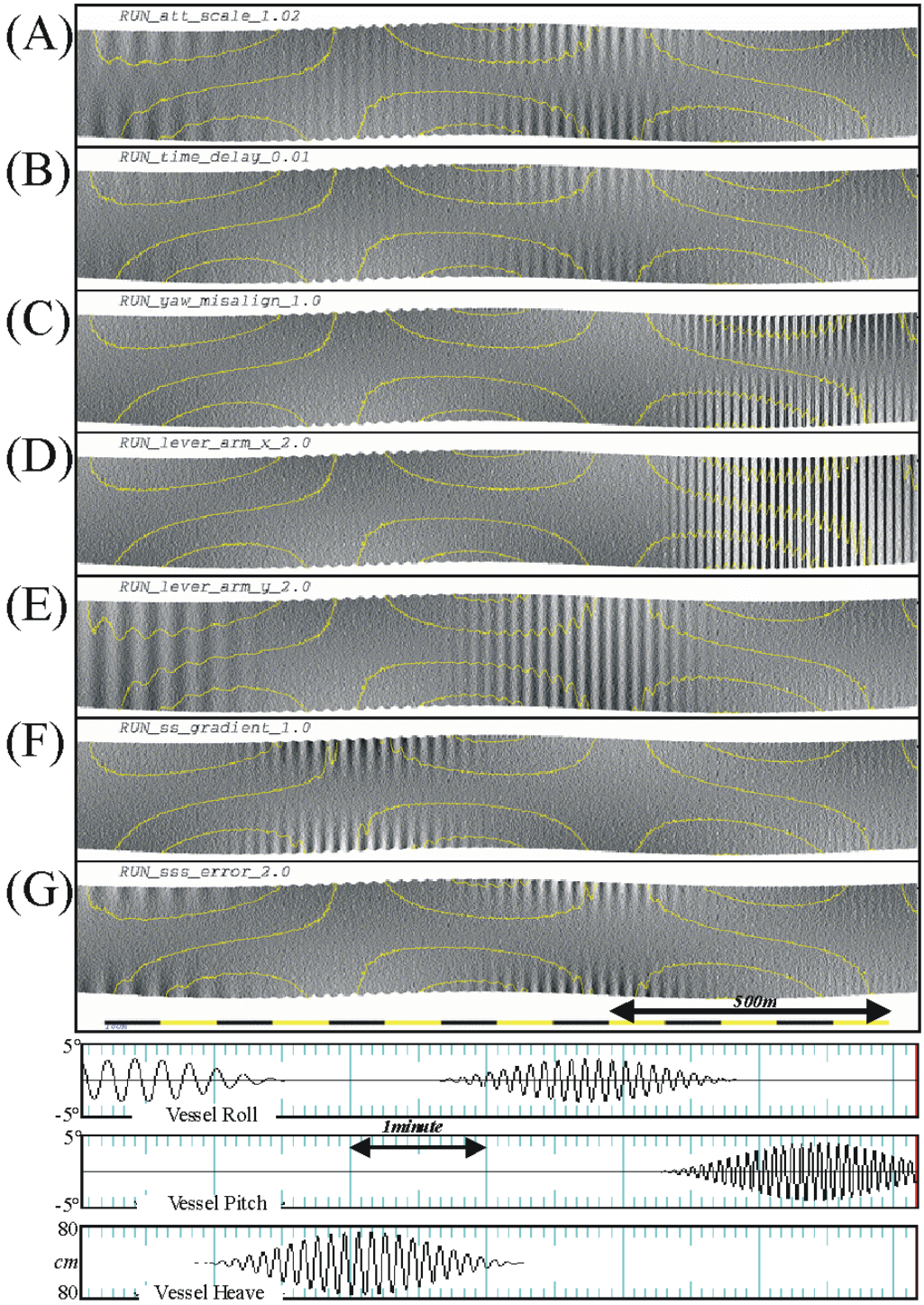

Figure 6*: examples of sun-illuminated terrain models derived from the output of a synthetic swath sonar (150° swath, roll-stabilized, 25m depth, 8 knots, seabed slopes in the range +/-1.0° with varying slope azimuths). All runs are subjected to a synthetic motion time series (lower three windows). Sun-illumination from the west and contoured at 1m intervals.*
Integration errors applied are: (a) scaled motion - 102% (b) delayed motion - 10ms, (c) cross-talk between roll and pitch – yaw misalignment of 1.0°, (d) X lever arm error – 2m, (e) Y lever arm error – 2m, (F) heaving through a surface sound speed gradient – 1/m/s per metre and (G) rolling with a surface sound speed error - 2m/s.

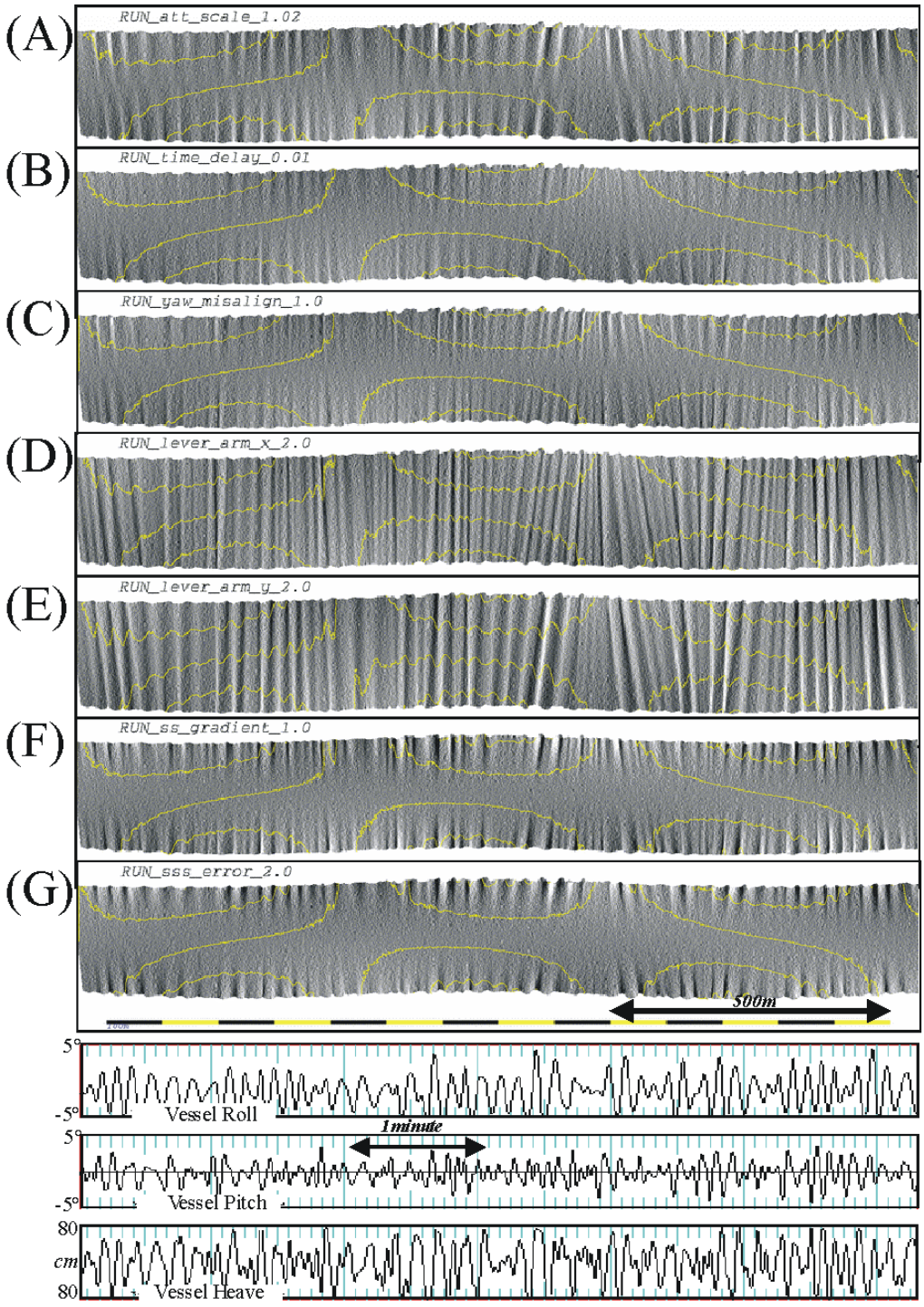

Figure 7*: examples of sun-illuminated terrain models derived from the output of a synthetic swath sonar (same parameters as figure 6)). All runs are subjected to an actual motion time series (lower three windows). Integration errors applied are the same as in figure 6.*

Using figures 6 and 7 as a guide, seven common dynamic error signatures will be examined by explaining the mechanism for generating each time varying error and then describing the characteristic identifying signature of that error type.

(A) Motion scaling problems

An historic problem with the older analog sensor outputs was a probability of a scale factor associated with the motion time series. This was prevalent with the sensors that would report the angles as voltages (10sin(angle)). Any loss of potential in the wiring would act as a scaling factor (not necessarily linear unfortunately).
Interestingly, scaling problems have been noted even in completely digital sensors (indeed several sensors allow you to program in a scaling factor for the angles to compensate for this). If this is the case, the magnitude of the error will scale with the magnitude of the angle (most noticeably roll).

The result (Fig. 6A, 7A) will primarily be a residual across-track oscillation of slope that simply correlates with the matching roll phase and an amplitude that is a fixed percentage of the roll. As manifested in the seabed topography, the roll error will result in a linear tilting of the across track profiles (Fig. 3 Type 1), which as viewed from sun-illuminated terrains will have zero magnitude at nadir, increasing linearly to the outer parts of the swath.

Scaling of the pitch, whilst probably present (built into this simulator) is unlikely to be very noticeable unless the seabed slopes are steep (in which case the predominantly horizontal errors induced result in apparent steps in the topography). If the heave is also scaled (again built into this simulator) each ping will be vertically offset by the difference between the true heave and delayed heave. One will thus notice a systematic rise and fall of all the beams together (Fig. 6A during heave packet, Type II of Fig 3).

In contrast to the next case, it should be noted that the error magnitude, whether in roll, pitch or heave scales only with the absolute magnitude of the actual motion and is unaffected by the period of the motion.

(B) Time delays in the motion sensor output

All digital motion sensors have an inherent internal delay due to the finite time to do the computations. Most motion sensors compensate for this by having a forward (normally quadratic) extrapolation algorithm so that the output solution is that predicted at the time of reporting. Additional delays possible can be attributed to the serial line transmission time and any time sitting in the input buffer of the integration CPU.

Data today are generally good to within +/- 10ms. The highest routinely used data output rate is at 5ms periods, but many sonar manufacturers' integration software prefers rates at intervals much longer than this (50ms for some systems). Where data rates are low, it is important that the integration software properly interpolate between sparse samples.

The importance of time synchronization depends on the rate of change of orientation. For a sinusoidal motion such as roll (R) of period T and amplitude A, the maximum rate of change occurs as the motion passes zero at a rate proportional to the amplitude and inversely proportional to the period:

$$R_t = A\sin(2\pi t / T)$$
$$\frac{\delta R_t}{\delta t} = \frac{2\pi A}{T}\cos(2\pi t / T)$$

Thus, for example, a typical wave period of 10 seconds with an amplitude of +/-3° provides a maximum rate of change of ~0.019° per ms. Thus a 0.1° error can occur with as little as 5ms motion time delay. For +/-75° systems this will exceed a 0.5% vertical error in the outermost beams.

Although all three motion sensor outputs, roll, pitch and heave would be delayed, the roll signature error would be the most notable. As with error A, one would experience a linear tilting of the swath (Fig 3. Type I), but in this case, it would correlate with the roll rate rather than the roll. In figure 6, whilst images A and B appear similar, one can notice that, although the roll energy packets present are of the same amplitude, in B, the ribbing is more pronounced for the shorter period motion as the rate of change of roll is higher.

As with A, there will be a pitch error, this time correlated with the pitch rate, but it is unlikely to be noticeable unless the fore-aft seabed slope is pronounced. And there could be a heave type error (Fig 3 Type II) if the resulting heave error magnitude is significant (as can be seen in figure 6B during the heave event).

(C) Imperfect alignment of the roll/pitch axes with the sonar reference frame.

Whilst the patch test examines misalignments of the motion sensor pitch and roll axes about themselves (static shifts in roll and pitch). It does not test for misalignment of these axes about the mutually orthogonal axis (heading). The gyro alignment in the patch test examines the alignment of the heading sensor, which in the past has usually been a physically separate unit such as a gyrocompass (Fig. 8). As a result a proper patch test heading alignment does not necessarily imply that the roll and pitch axes are properly aligned in yaw.

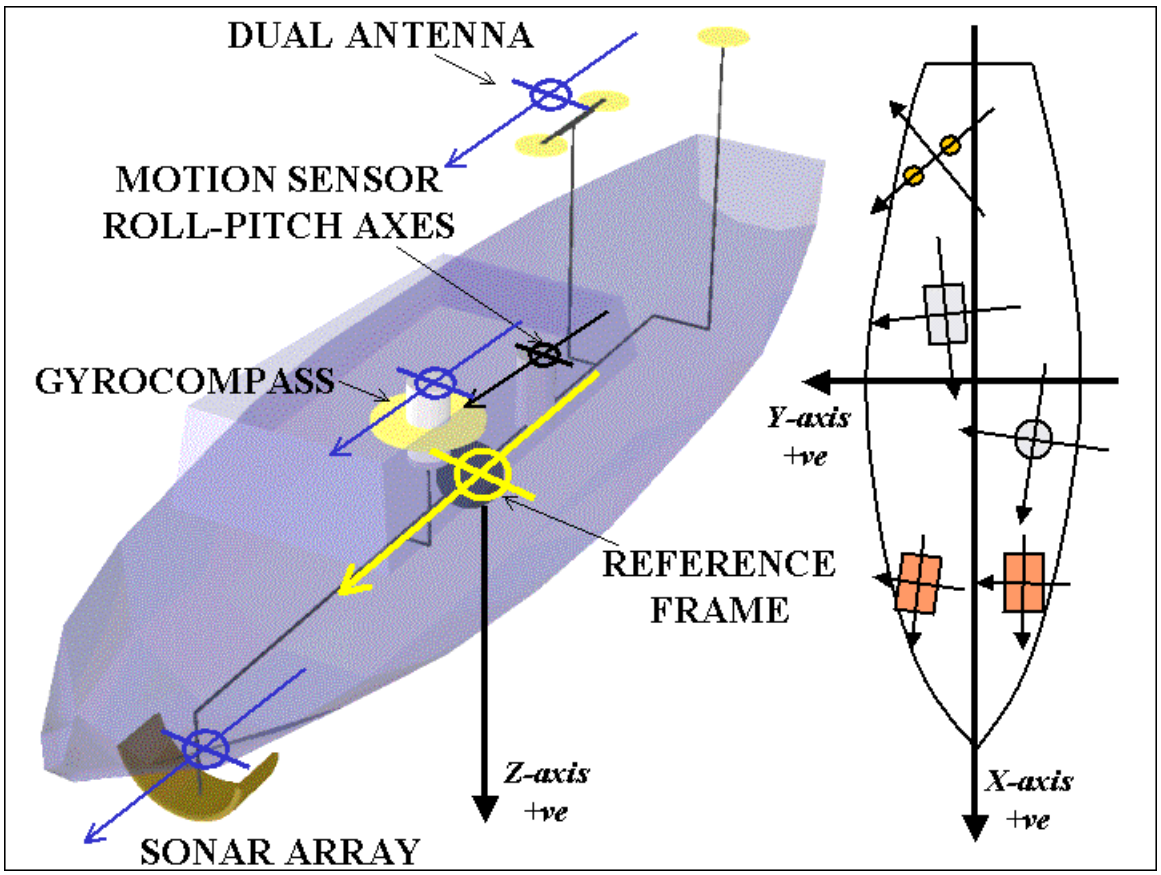

Figure 8*: showing the relative yaw alignments of all the different sensors with respect to the ships reference frame*

More recently, motion sensors that integrate dual GPS antenna heading have appeared (Applanix POS/MV; Seatex Seapath). Depending on how the integration is done, altering the heading alignment may or may not implicitly alter the alignment of the roll and pitch axes.

For some sensor packages, a calibration procedure is established where the alignment of the GPS antenna pair with respect to the inertial measurement unit (IMU) axes is explicitly solved (POS/MV). In this case when a heading misalignment is entered into the IMU software, it rotates the roll and pitch axes with these. Other integrations however are looser in that the GPS antenna axis alignment with the ship reference frame is treated as separate to the roll and pitch axes Z alignment.

Should roll and pitch be reported about axes that are offset around the Z axes from the sensor that one wishes to describe, there are both dynamic and static angular errors are introduced.

Dynamic Angular error

A misalignment around the Z-axis of the roll and pitch axes will cause cross talk between the two axes as described in the following equation:

OR : observed roll TR : true roll
OP : observed pitch TP : true pitch
E : yaw misalignment angle

$$\sin(OR) = \cos(E)\sin(TR) + \sin(E)\sin(TP)$$

$$\sin(OP) = \cos(E)\sin(TP) - \sin(E)\sin(TR)$$

There are two consequences here:
(1) - In the absence of motion on the other axis, the signal is attenuated by the cosine of the yaw alignment error. This might be confused with an attitude scaling error A.

(2) - When there is motion on the other axis, there is cross talk which leaks through according to the sine of the error. The most sensitive consequence will show up as a dynamic roll error (Fig. 3 Type I) that correlates with pitch

Recalling the shape of sine and cosine functions for small angles, it is clear that the crosstalk is the main concern as a 1° misalignment will result in only 0.05% attenuation of roll but up to 1.75% of pitch crosstalk. Thus, a roll error that correlates with pitch (Fig 6 C) will be the most noticeable characteristic of a motion time delay

Static Angular Error

Whilst the periodic undulation due to pitch bleeding into roll will be the dominant signature noted, it should be realized that if the vessel runs with a constant pitch trim offset, this will be equivalent to a small roll bias. Thus if the trim is a function of speed, one will see an apparent roll bias that changes with speed through the water. The reverse is true in that a static list of the vessel will translate into an apparent pitch bias. In both cases, if this is suspected, the patch test needs to be rerun after Z rotation of the roll and pitch axes.

(D,E) Errors in relative offsets of sensors in the ships coordinate system.

If the location of sensors within the ships coordinate system is incorrectly reported (for example signs are often confused), this will result in incorrect sensor location prediction. The errors resulting are positional in nature as no angular misalignments are involved. These position errors will be manifested as both static and dynamic errors.

Static:

Position sensor offset errors will translate into predominantly static vertical and horizontal biases. The Y shift will primarily be a static across track shift (slightly modulated by the roll). The Z shift has minimal horizontal effect (unless large static lists or trims biases are common) but is particularly critical if the Z solution is derived from the RTK at the antenna. Also, if there is a constant trim or list in either pitch or roll then this will translate into a static vertical shift in the predicted position of the transducer (a DC component to the induced heave).

The X component however, has more far reaching issues as it will provide predominately static fore-aft displacement. If it is undetected, it will confuse the conventional time delay and pitch patch test and thus result in imperfect solutions. If the time delay is miscalculated, there will be an apparent change in the time delay with speed. Similarly, if the pitch displacement is miscalculated (due to confusion with the X component) then the pitch alignment will appear to change with depth.

Dynamic:

The most significant dynamic contribution to the error budget is the calculation of the induced heave due to lever arm between the reference point and sonar. The induced heave error IH_{err} would depend on the lever arm errors (dX, dY, dZ) and magnitude of the roll and pitch (r, p):

$$IH_{err} = -dX\sin(p)+dY\sin(r)\cos(p)+dZ(1-\cos(r)\cos(p))$$

In this case false X and Y (and to a much lesser extent Z) lever arms translate directly into apparent heave errors at the sonar. These errors are clearly dynamic. Where the ping rate is much shorter than the characteristic roll or pitch period, the magnitude of the induced heave error would be almost identical for all beams in that swath. This will thus be manifested in the data as an in-phase lifting and falling of all the beams (Fig. 3 Type II).

Due to the order of rotation convention, X lever arm errors will show up directly correlated with pitch (Fig. 6 and 7 D). Similarly Y lever arm errors are predominantly correlated with roll (Fig 6 and 7E), but would have a small pitch influence (pitch would only be important at large values where cos(p) deviates significantly from 1).

(F) Vertical motion close to or in a sound speed gradient.

Any difference between an erroneous surface sound speed V_{err} and the correct sound speed V_{corr} results in an erroneous beam steering angle θ_{err} for those beams steered away from boresite :

$$\theta_{err} = \sin^{-1}\left(\frac{V_{err}}{V_{corr}}\sin(\theta_{corr})\right)$$

(θ_{corr} is the desired angle)

For a level receive array in a water mass of fixed sound speed error (at all depths), the result is a static bias similar to a conventional refraction artefact. More usually however, the sound speed error is restricted to a thin layer at the surface and thus below this layer the ray will refract back to direction parallel to the intended ray path. This is because even though the predicted sonar-relative angle is wrong, the Snell's constant is actually correct. This depends on the array being level and thus the sonar relative angles are also relative to the local level. This can be seen by rearranging the equation above:

$$\frac{V_{err}}{\sin(\theta_{err})} = \frac{V_{corr}}{\sin(\theta_{corr})}$$

As the predicted and actually trajectories are parallel for the majority of the ray path, for this special case, of level receive arrays, the errors are surprisingly minimal (Cartwright and Hughes Clarke, 2002).

But for barrel arrays where no beam steering is occurring there is no initial beam pointing angle error and thus if the sound speed returns to a known level at depth, the angular error manifests itself below the erroneous layer depth (because the original Snell's constant was not correct). As a result the ray path in the majority of the water column is not parallel to the intended path. This will result in a conventional refraction bias.

Surface sound speed errors are a particularly common situation that occurs in river or estuaries where there is a strong near-surface sound speed gradient. If the transducer oscillates vertically within a strong sound speed gradient (Fig. 9), the sonar-relative water column structure changes dynamically in phase with the vertical motion (the vertical motion is reasonable approximated by the heave and induced heave at the sonar for areas with insignificant wave action).

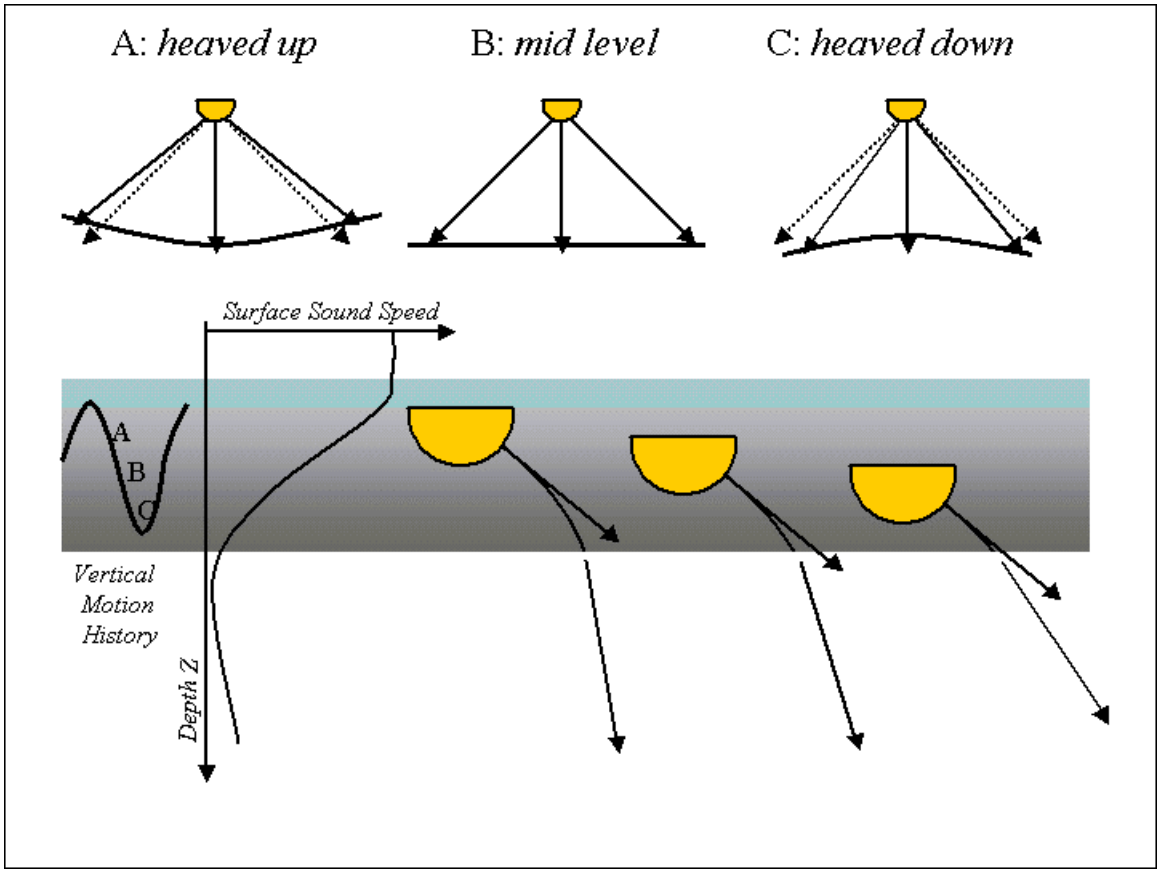

Figure 9*: showing the consequences of heaving a barrel array through a velocity gradient.*

The end result is that one will have a refraction artefact symmetrical about nadir, with both sides either curled up or down, that oscillates in magnitude and phase as the transducer moves up and down (Fig. 9). This will look like Type IV (Fig. 3). It is clearly distinct from either Type I ribbing (A, B or C) as the outer beam errors are in phase. And it is distinct from Type II ribbing (D or E) as the near nadir beams do not show motion. When examining the result in the data (Figs. 6 and 7 F) one sees ribbing that correlates with vertical displacements of the sonar. Superficially it looks similar to Type I ribbing as there is no artefact at nadir, but on closer detail it is apparent that the sun shading is in phase on either side.

(G) Rolling with an imperfect surface sound speed

Error F assumes an oscillating sound speed error. More commonly, the surface sound speed is simply wrong. As explained above, for a flat line array, as long as the sound speed structure returns to the old value at a shallow depth, the angular consequences are minimal. But as soon as the receive array is no longer level (due to roll or mounting angle ϕ) the erroneous sonar-relative steering angle is derived thus:

$$\theta_{err} = a\sin\left(\frac{V_{err}}{V_{corr}}\sin(\theta_{corr} - \phi)\right)$$

And therefore the Snell's constant is not preserved:

$$\frac{V_{err}}{\sin(\theta_{err} + \phi)} \neq \frac{V_{corr}}{\sin(\theta_{corr})}$$

Thus the resulting angular error depends on the roll magnitude and sign and therefore will be dynamically related to the motion time series. As the magnitude of the steering error depends on the sonar-relative steering angle desired (zero at boresite, growing with obliquity), if the sonar itself is rolling, then the required steering to a vertically referenced angle changes continuously. Therefore the magnitude of the error at that vertically referenced angle changes as the array rolls. As shown in figure 10, when the sonar is up on one side, the beam steering error on that side is less, whereas it is greater on the rolled down side.

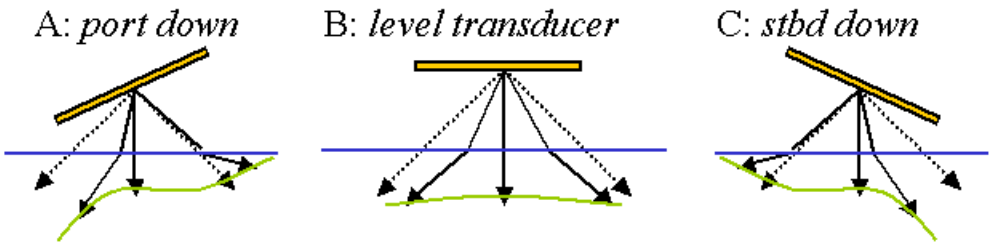

Figure 10*: showing the consequences of rolling a flat line array with a false surface sound speed*

Combining the beam steering errors with the correcting influence of the step back in sound speed below, one thus has an upward refracting on one side at the same time as one has a downward refracting environment on the other side (Fig. 10). The end result is a tilting from side to side that has a non-linear curvature on each side. Each side in isolation would look similar to F, but unlike F, the two sides are out of phase from side to side. The resulting wobble is thus a unique type (Fig 3 Type III). As seen in figs. 6 and 7 G, the error correlates with roll.

This nonlinear tilting of each side is at first glance, quite similar to Type I ribbing error (A, B or C). As it correlates with roll, this makes this artefact quite difficult to distinguish from a simple roll-scaling problem (A). The best way to distinguish the two is to compare the across track slope derived using innermost beams against the slope derived from using the outermost beams. The two should be the same for roll scaling, but different for the beam steering error case (as the refracted profile is curved).

The seven most common dynamic motion artefacts have been described above. There are however, several other situations in which dynamic motion artefacts can be generated including the obvious ones (motion not applied or motion applied backwards). An example of a more subtle one is pitch steering using the incorrect sign. However, all of these errors assume a rigid lever arm between motion sensor and sonar. If this is not the case, then other, possible motion correlated angular errors may show up.

Deformation of the lever arm between orientation sensor and sonar

This is most prevalent for pole-mounted systems. Stress on the mounting frame will depend on the speed through the water and the rate of rotation of the pole. Thus one may expect angular deformations that are speed dependent, (including high frequency (1+ Hz) vibrations) and also angular deformations that result from the lateral drag of the pole as the vessel rolls (and thus the errors might appear to be motion driven). Deformation errors are predominantly angular in nature, and thus may be confused with other motion-correlated errors. However, the most notable characteristic is often a pseudo-random variation effect, together with a high frequency noise.

There is little one can do with mount rigidity problems in post processing as the cause cannot readily be inferred. In real-time, the solution, of course is to replace or strengthen the mount. Placing the motion sensor with the sonar on the mount can help but leads to problems with static trim and list and of course the danger of loss of sensor.

Improper Integration Software

Even if the sensor relative alignment, offsets and timing are actually perfect, there may still be dynamic motion residuals if the integration software used does not properly account for the full system geometry. If simplifying assumptions are made such as for example: assuming the steered beam vector can be approximated by the intersection of

tilted planes rather than cones; or failing to account for yaw changes over the receive cycle, the result may have a time varying error. These errors are the most frustrating, as they are a result of the integration software itself and not the sensors. There is a proliferation of 3rd party integration software today that tries to handle all sonars systems on the market. If these do not fully take into account the uniqueness of each system type (not always well explained for proprietary reasons in the manufacturers documentation) then residual errors will remain.

Extraction of Error Characteristics and Classification of Residual Type

For those errors that are primarily driven by motions in the ocean wave spectra, errors such as those described above manifest themselves as a periodic undulation of the swath bathymetric data (Fig. 3A). For example, if the characteristic wave period is ~8 seconds, a vessel running at 10 knots (5m/s) will experience ~40m wavelength undulations in the swath corridor oriented roughly orthogonal to the ships track.

These undulations are easily apparent in sun-illuminated terrain models (as long as the sun-illumination hasn't been oriented specifically to be parallel to the strike of the undulations, as so often happens to hide the effect). But if we are to identify the cause of the undulations, there remains a requirement to correlate the undulation with the matching motion time series. We thus need to develop a method of extracting the characteristic of the resulting bathymetric undulation and plotting this as a time series along with the motion time history.

There are two main characteristic types of undulations:

- those in which the outer edges of the swath rise and fall (Types I, III and IV) and
- those in which the whose swath rises and falls (Type II)

Both these characteristics may be extracted from the bathymetric data with care. There is always the danger that the seafloor is in fact undulating in this manner due to natural morphology (bedforms or bed rock ridges). Thus a reasonably reliable method of identifying whether the undulations are natural or an artefact needs to be developed.

<u>Use of across track slope as an indicator of time varying roll errors</u>

For the oscillating swath profile, a time series of the average across-track slope will provide a combination of the motion residual and the regional across-track slope. The average across track slope can simply be derived by performing a linear regression on the across-track and depth values for a single ping.
If one can identify an area in which the genuine seafloor across-track slope only changes over time constants far longer than the ocean wave period (e.g. one minute, ~240m at 8 knots) then one can high-pass-filter the time series of across-track slope to extract only that component with periods in the ~ 4-16 second range.

Use of across track average depth as an indicator or time varying roll errors

Similarly for the systematically rising and falling swath, an average of all the beams in the swath will amplify relief that is in phase for all beams. Again, there may be regions of the seabed where one is steaming orthogonal to the crests of short wavelength relief, but again by using regions with only long wavelength relief (e.g.: unconsolidated fine-grained sediments), a high-pass-filtered version of this time series of average depth will contain an indicator of the likely artefact.

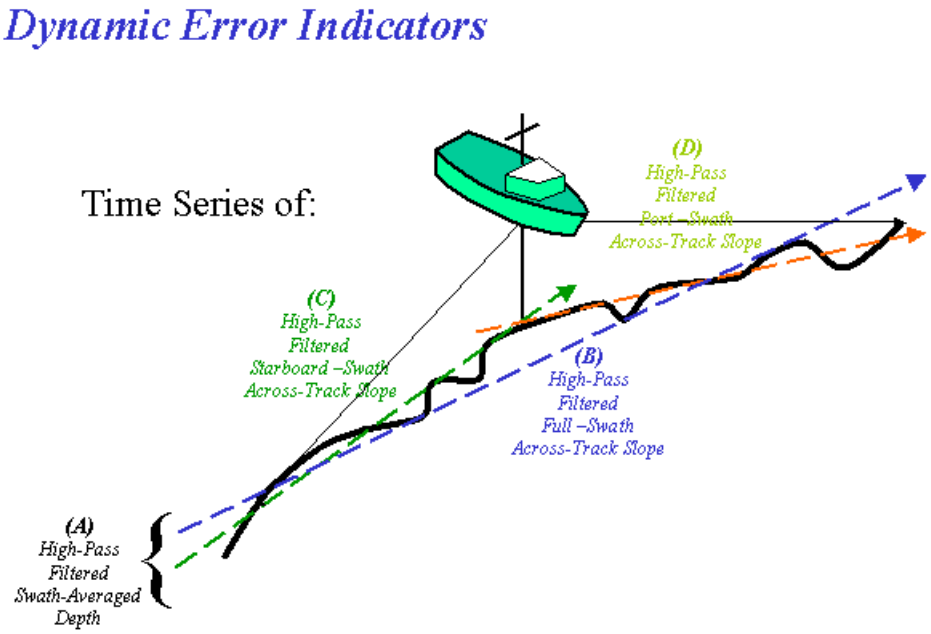

Figure 11*: extraction of dynamic error residuals*

In both cases, one needs to be sure that the ribbing does not relate to natural seabed morphology. It is extremely unlikely that natural ribbing would be exactly orthogonal to the ships track. If not exactly orthogonal, then the natural ribbing will in part be expressed as a roughness in the across-track profile. Such roughness, if present, can be detected by a larger than usual residual of the linear regression. An example of this can be seen by examining a time series of the residuals (Fig 12) derived from the swath sonar data shown in Fig. 1 as the vessel steams from P to Q.

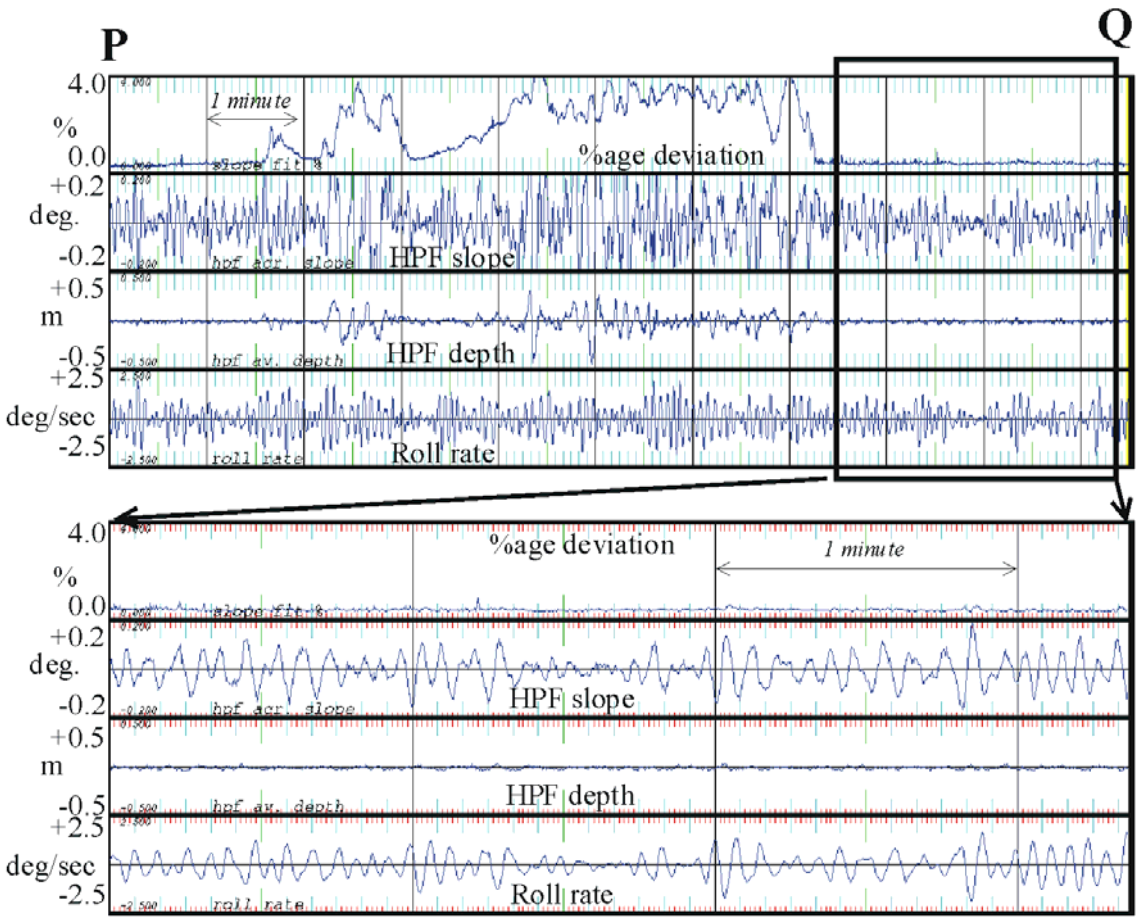

Figure 12*:*
upper - time series from point P to point Q in figure 1 and
lower - zoom window within that of:

- *Percentage deviation of swath data from linear regression*
- *High pass filtered across track slope*
- *High pass filtered average depth*
- *Roll rate (at average time of beam receive)*

From figure 12 (upper) one can see that within the line from P to Q (shiptrack illustrated in Fig. 1), there is a period in which the percentage deviations abruptly rise up. From the sun-illuminated terrains in figure 1 it can clearly be seen that this correlates with the time when bedrock or reefs are present within the seafloor data. During that same time period the across-track slope and average depth indicators have a strong false signature due to the natural topography.

Regions of flat seafloor are seen to exhibit a uniformly low normalized deviation (in this case < +/-0.5% RMS deviation). This deviation is a combination of bottom detection noise and 2nd order curvature of the profile (either due to geology or a slight refraction bias). Where natural roughness is seen, the deviation jumps abruptly. Such regions should be excluded from the data analyses.

As the high pass filter used to extract the bandwidth limited signatures is implemented herein using a time domain weighted filter, any data within half the length of the filter from a rough swath profile must be treated as contaminated. The length of the filter depends on the longest motion period that one wishes to preserve. Typically the filter length is ~4 times longer than the longest characteristic period. For these analyses, only those filtered samples in which more than 90% of the deviations within the filter window were below 0.5% were used.

Complications due to irregular seafloor sampling

One is trying to use a bandwidth limited time series of the seabed observed morphology as an indicator of the time series of the artefact. This assumes that the seabed morphology is being sampled in a similar systematic manner. Unfortunately that is not exactly the case for imperfectly stabilized swaths.

In both average depth and average slope cases, care has to be taken that one is not misled by the irregular seabed sampling that can occur with non-roll or pitch stabilized swaths. For example if the swath is not roll stabilized, (Fig.13 upper) the average depth will migrate up and down when rolling across a regional slope.

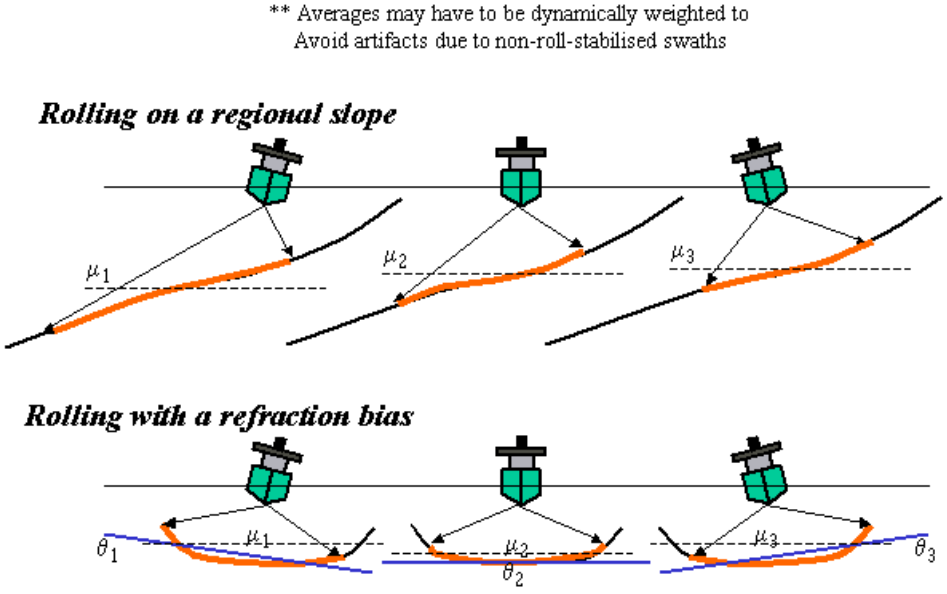

Figure 13*: showing the problem of extracting average slope and average depth parameters from non-roll stabilized swaths that are either on a slope (upper) or imperfectly refraction corrected (lower)*

A second problem routinely encountered is when analyzing non roll-stabilized data that has a slight refraction bias. As the swath rolls, the more-distorted outer beams are sequentially sampled to a greater degree on each side as the swath rolls toward that side (Fig 13 lower). This results in both an apparently oscillating average depth, but more significantly an oscillating apparent average slope neither of which are due to imperfect integration.

To avoid either of these problems, one should utilize those solutions only within a roll stabilized sub sector of the swath that is always occupied.

A similar problem occurs with the average depth if one has a system that is not pitch stabilized and one is steaming up a regional slope (Fig. 14). In this case, the time series of average depth will appear to be irregular due to sampling respectively uphill of or downhill, of the depth below the vessel. In this case, steep slopes should be avoided as part of this type of analysis.

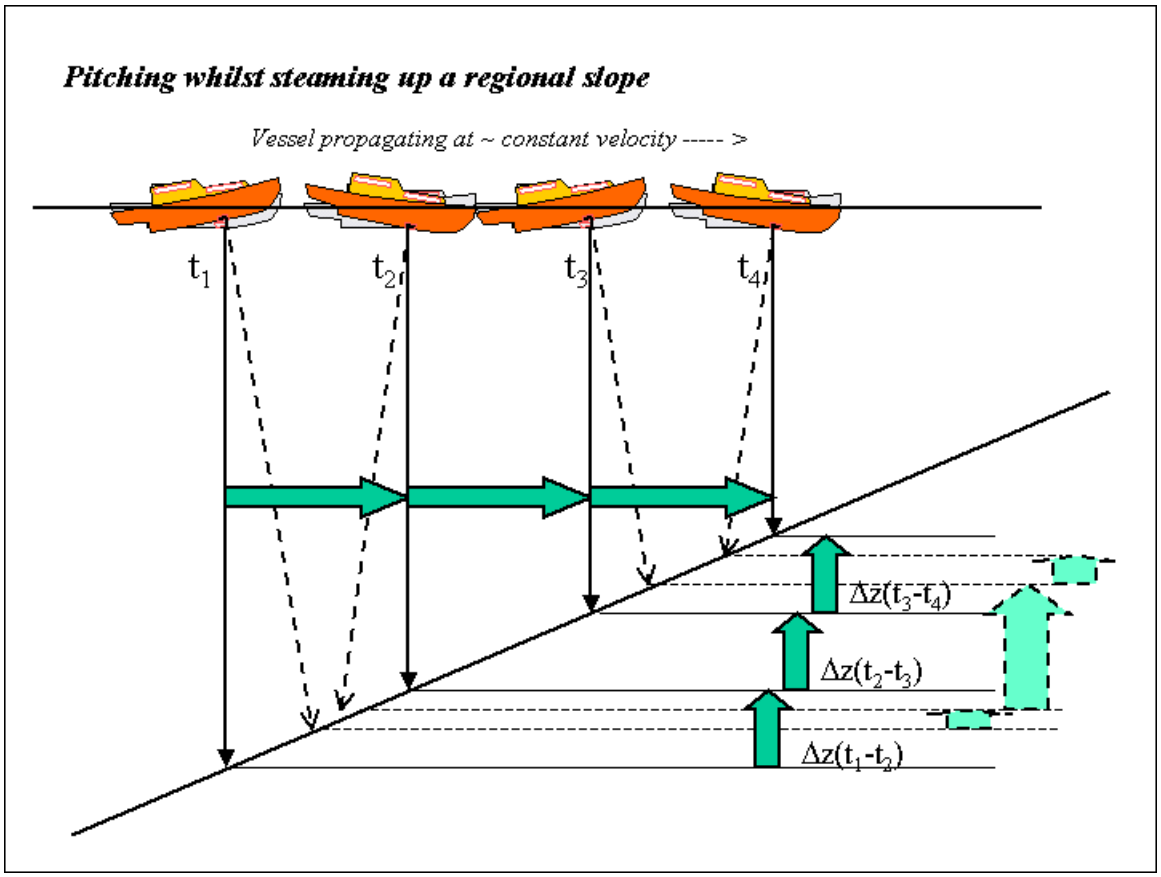

Figure 14*: showing the apparent irregular bathymetry sampled as a time series when pitching on a regional slope that is actually smooth.*

Similarly for yawing on a regional slope, one's estimate of the average across track slope will oscillate as the strike of the instantaneous ping varies (Fig 15).

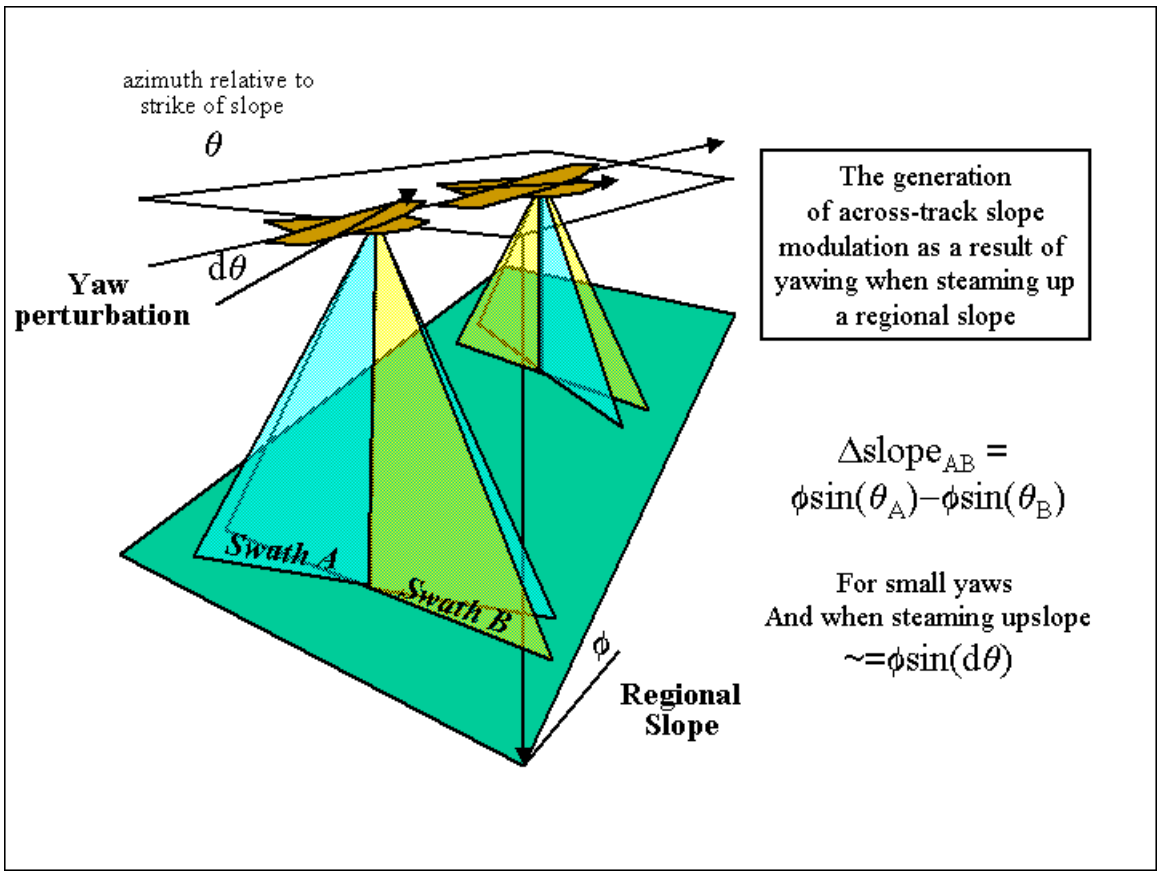

Figure 15*: cartoon illustrating the apparent oscillation of the across-track seafloor slope when yawing.*

The apparent slope expressed in the instantaneous across track profile depends on the regional slope and the yaw perturbation. Again, excessive yawing (at periods similar to the roll and pitch periods) whilst steaming up slopes should be excluded from the analyses.

Quick-Analysis Method

Based on examination of the resulting bathymetric data and its correlation to the driving signatures (as outlined above), a guide is developed that might allow the on-line operator to most effectively separate out the principal cause of the observed residual.

In all cases one is looking for a correlation between one (or more) of the driving signatures and either the high pass filtered (HPF) across-track slope or HPF average depth. The most effective way of visually assessing a correlation is to examine a cross plot. Figures 16A and B show cross plots for all the examples generated in Figure 6 and 7.
For each survey line the following cross plot displays are used:

	X value	X range		Y value	beam sector	Y range
i.	Roll	(+/-5°)	v.	HPF full slope	-70° to +70°	(+/-0.2°)
ii.	Roll	(+/-5°)	v.	HPF inner slope	-45° to +45°	(+/-0.2°)

iii.	Roll Rate	(+/-2.5°)	v.	HPF slope	-70° to +70°	(+/-0.2°)
iv.	Pitch	(+/-5°)	v.	HPF slope	-70° to +70°	(+/-0.2°)
v.	Roll	(+/-5°)	v.	HPF depth	-70° to +70°	(+/-0.5m)
vi.	Pitch	(+/-5°)	v.	HPF depth	-70° to +70°	(+/-0.5m)
vii.	Heave	(+/0.5m)	v.	HPF slope port	-70° to +0°	(+/-0.2°)
viii.	Heave	(+/0.5m)	v.	HPF slope stbd.	-0° to +70°	(+/-0.2°)

All these are plotted in Fig. 16, from which it can be clearly seen that the signature of each artifact is distinct:

(A) Attitude Scaling	Type I	-	HPF slope correlates with roll (slope is same for inner and outer swaths)
(B) Time Delay	Type I	-	HPF slope correlates with roll rate
(C) Yaw Misalign of pitch/roll axes	Type I	-	HPF slope correlates with pitch
(D) X lever arm error	Type II	-	HPF average depth correlates with pitch
(E) Y lever arm error	Type II	-	HPF average depth correlates with roll
(F) Surface Sound Speed Gradient	Type IV	-	port and starboard HPF slope correlate in equal and opposite directions with heave (transducer depth)
(G) Surface Sound Speed Error	Type III	-	HPF slope correlated with roll (*and* slope of inner +/- 45° is much flatter)

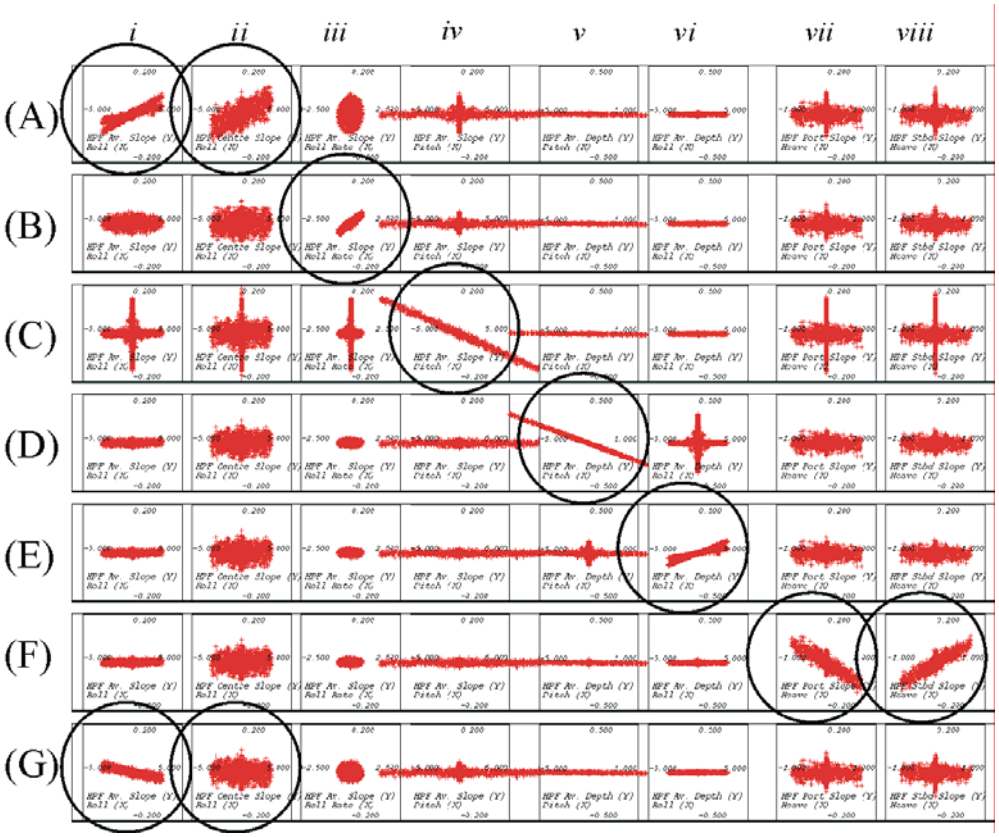

Figure 16a*: synthetic motion simulations – Cross plots (as described in text, including axes labeling) for the 7 different types of artefact shown in Figure 6.*

.

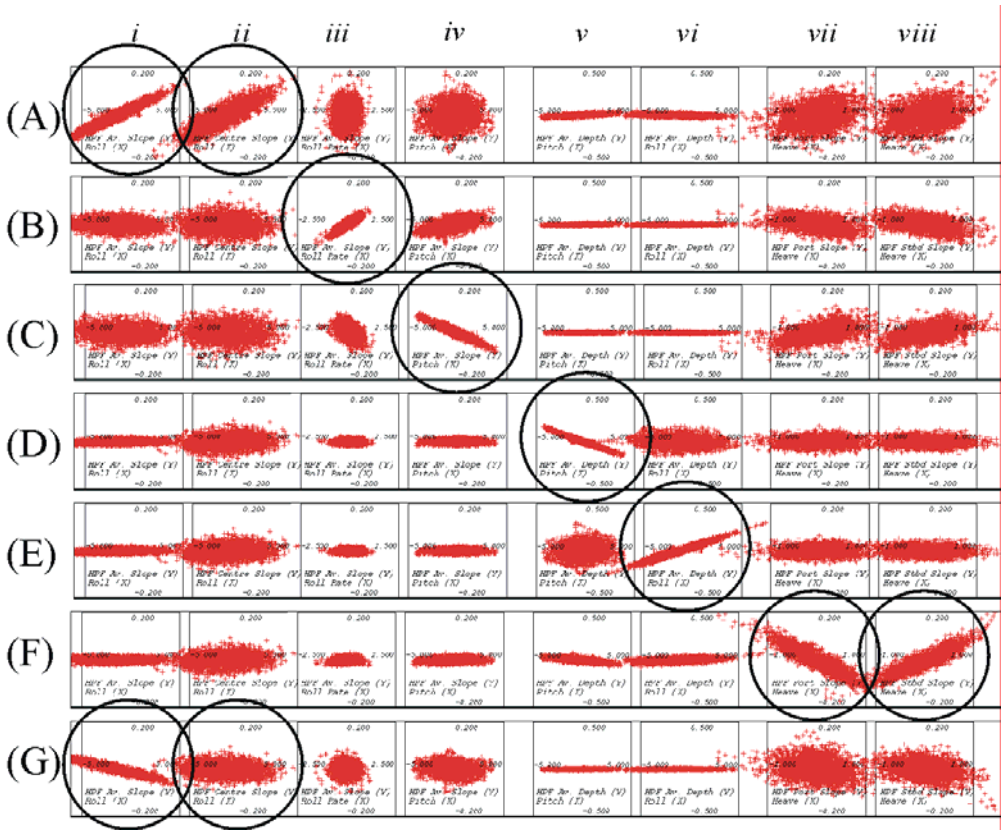

Figure 16b*: : real motion simulations – Cross plots (as described in text) for the 7 different types of artefact shown in Figure 7..*

In all cases, the slope of the cross plot correlation is indicative of the magnitude of the underlying systematic bias.

Dual Head Complications

Whilst all the examples shown here are for errors common to a single headed sonar system, those errors need not be shared for both sides of a dual headed system. For example, lever arms and/or yaw misalignments are often different for each head. Thus it is quite conceivable that the wobble may be constrained to a single side, or even worse, each side may have a unique wobble.

Today, dual headed systems usually share a common source of orientation, a common clock and a common sound speed structure so that attitude scaling, motion delays and refraction artifacts should be common to both of the heads.

Coping with more than one source of error

Whilst each of these artefacts is unique in isolation it becomes far more difficult to handle them when more than one is present. Some are clearly independent such as those that generate Type I (ABC) and Type II (DE) and thus they could be analysed

simultaneously. A complication would be if heave scaling was present. There is no consequential difference between a Type II error from a scaled roll and pitch and the same scaling of the lever arm in Y and X.

Type IV (F) is the most unambiguous as it's signature is unique. It could thus probably be identified in the presence of any of the other errors. Distinguishing G (Type III) and any of the Type I errors is much harder. As noted above identifying the nonlinear curvature in G by using inner and outer swath slopes is seen as the most promising.

In all cases, the analyses would realistically be progressive, with the error source causing the largest signature being eliminated first and then analyzing for the presence of other less consequential errors.

Example Application

The example used is shown in Figure 1 before and after post-processing analysis and correction. For the shiptrack from location P to Q, the time series of the high-pass-filtered across-track slope and average depths have been extracted and plotted against the roll rate in figure 12. By selecting only data in which the percentage deviations are small (Fig. 12 lower) one can visually appreciate a strong correlation of the across track slope against the rate of change of roll suggesting a motion time delay problem.

To quantitatively assess the nature of the ribbing in the data, we now perform the cross-plot analysis. Figure 17 shows the identical series of cross plot displays exhibited in Figure 16. The upper plot is before adjustment where one clearly sees a tight correlation in the iiith window indicating the presence of a motion delay. Interestingly, the slope of the cross plot correlation is reversed from that in Figure 16 where the synthetic delay was positive. This indicates that the delay is negative (that is the motion is being predicted too far into the future). By analysis of the slope of the cross plot we can estimate that the delay is approximately –20ms. If we then shift the motion time series and redo the full sensor integration calculation we can remove most of the wobble signature in the data (Figure 1b).

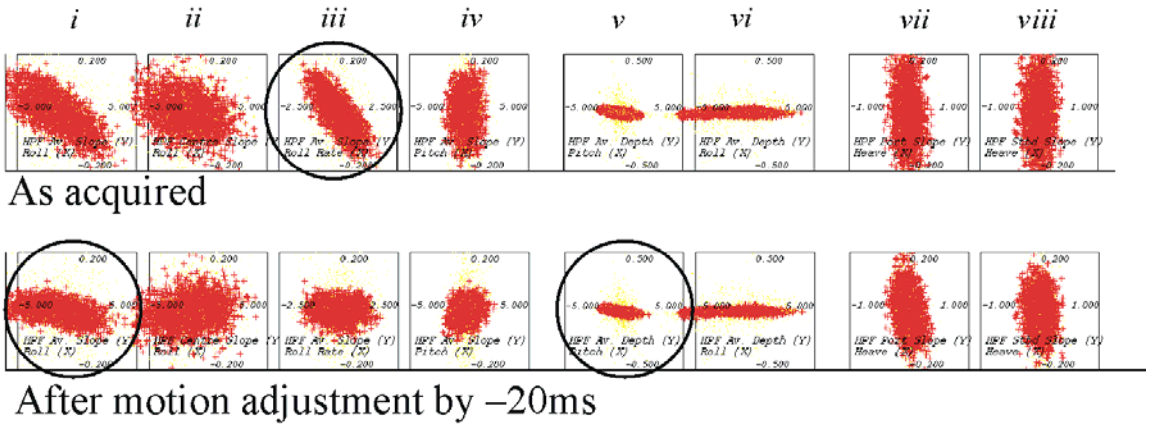

Figure 17*: Cross plot analysis of the swath sonar data used to make Figure 1. plot axes values and scales are described in text Top, before adjustment as collected. Bottom, after adjustment.*

Interestingly, after adjustment (Fig 1b) one can now see a smaller wobble error that is actually within a subset of the total swath. This is a unique and unusual problem where the edges of the transmit beam patterns for the inner sector of this EM1002 were too weak (a hardware fault). The result was a wobble of edges of the inner sector (+/-50°), which actually correlates with the roll. Referring back to the X plots in Figure 17 (lower), after removal of the time delay problem, one now sees a much weaker but notable correlation between slope and roll that is a result of this inner sector wobble.
Also in the Fig. 17 (lower) one sees just a suggestion that the X lever arm from heave sensor to sonar may have a small error.

The presented example illustrates the practical applicability of this method for analysis of swath sonar data. Is should be noted that in this example, the imperfect data were already acceptable for the purpose of survey (equivalent to IHO order 2). Nevertheless, fine scale seabed relief, resolvable by this sonar was being contaminated by a systematic bias that resulted in a notable wobble. The post processing analysis described in this paper was clearly able to identify and remove that effect.

Conclusions

As we have continued to improve both the quality of ancillary sensors and the power of visualization, the importance of dynamic motion residuals has risen to the forefront. Significant concern is currently being raised by clients with respect to these periodic artefacts. This is because, whilst they are within the absolute accuracy specifications, they are larger than the smallest vertical scale of natural feature that can usually be resolved (commonly 0.25 to 0.5% of depth (Hughes Clarke et al., 1996)) and thus they appear detrimental to the data quality. Whilst a contractor can argue that these data are strictly within specification, it is clear that such artefacts can certainly not be described as a random error component, their presence being clearly correlated with ship motion and thus they should be removable.

Through the methods outlined it can be shown that these artefacts are invariably systematic and diagnosable through analysis of the acquired contaminated data. Ideally, these artefacts would be identified in short-order in the field and the cause remedied. The reality is that imperfect field processing often misses these fine scale features. Using the analysis method described herein the signature of 7 of the most common sources of wobble can clearly be distinguished. Therefore, as long as the full motion time series and sonar relative angles are retained, by fine scale tuning of the integration in post-processing, they may be removed from the data set.

Acknowledgements

This work has benefited immeasurably from the open provision of problematic data by a large number of survey agencies. Most notably data collected by the Canadian Hydrographic Service, the Geological Survey of Canada, the U.S. Geological Survey and the Geological Survey of Israel have been used in the development of this analysis method.
This research has been supported through the active sponsorship of the Chair in Ocean Mapping. Sponsors include the Canadian Hydrographic Service, the U.S. Geological Survey, the U.S. Naval Oeanographic Office, Kongsberg Simrad, the University of New Hampshire, the State University of New York and CARIS Ltd..

References

Cartwright, D. and Hughes Clarke, J.E., 2002, Multibeam surveys of the Frazer River Delta, coping with an extreme refraction environment: Canadian Hydrographic Conference Proceedings CDROM.

Herlihy, D.R., Hillard, B.F., Rulon, T.D., 1989, National Oceanic and Atmospheric Administration Sea Beam "Patch Test" Manual: Ocean Mapping Section, Office of Charting and Geodetic Services, NOS, 34 pp.

Hillard, B.F., Rulon, T.D., 1989, National Oceanic and Atmospheric Administration HydroChart II system "Patch Test" Manual: Ocean Mapping Section, Office of Charting and Geodetic Services, NOS, 35 pp.

Hughes Clarke, J.E., Mayer, L.A. & D.E Wells. 1996. Shallow-water imaging multibeam sonars: A new tool for investigating seafloor processes in the coastal zone and on the continental shelf. Marine Geophysical Research, 18: 607-629.

Hughes Clarke, J.E. 2000,Acoustic Seabed Surveying – Meeting the new demands for Accuracy, Coverage and Spatial Resolution Geomatica, v.54, no.4, p.473-413.